Frontiers of Physics
https://doi.org/10.1007/s11467-019-0923-2
Front. Phys.
15(1), 13601 (2020)

RESEARCH ARTICLE

Modulation of the electronic states of perovskite $SrCrO_3$ thin films through protonation via low-energy hydrogen plasma implantation approaches

Meng Wu[1], Shanquan Chen[2], Chuanwei Huang[2,†], Xing Ye[3], Haiping Zhou[3], Xiaochun Huang[4], Kelvin H. L. Zhang[4,‡], Wensheng Yan[5], Lihua Zhang[6], Kisslinger Kim[6], Yingge Du[7], Scott Chambers[7], Jin-Cheng Zheng[1], Hui-Qiong Wang[1,§]

[1] *Fujian Provincial Key Laboratory of Semiconductors and Applications, Collaborative Innovation Center for Optoelectronic Semiconductors and Efficient Devices, Department of Physics, Xiamen University, Xiamen 361005, China*
[2] *Shenzhen Key Laboratory of Special Functional Materials, College of Materials Science and Engineering, Shenzhen University, Shenzhen 518060, China*
[3] *School of Materials and Energy, University of Electronic Science and Technology of China, Chengdu 611731, China*
[4] *State Key Laboratory of Physical Chemistry of Solid Surfaces, College of Chemistry and Chemical Engineering, Xiamen University, Xiamen 361005, China*
[5] *National Synchrotron Radiation Laboratory, University of Science and Technology of China, Hefei 230029, China*
[6] *Center for Functional Nanomaterials, Brookhaven National Laboratory, Upton, NY 11973-5000, USA*
[7] *Physical Sciences Division, Physical and Computational Sciences Directorate, Pacific Northwest National Laboratory, Richland, WA 99352, USA*
Corresponding authors. E-mail: [†] *cwhuang@szu.edu.cn,* [‡] *Kelvinzhang@xmu.edu.cn,* [§] *hqwang@xmu.edu.cn*
Received July 20, 2019; accepted August 15, 2019

Hydrogenation of transition metal oxides offers a powerful platform to tailor physical functionalities as well as for potential applications in modern electronic technologies. An ideal nondestructive and efficient hydrogen incorporation approach is important for the realistic technological applications. We demonstrate the proton injection on $SrCrO_3$ thin films via an efficient low-energy hydrogen plasma implantation experiments, without destroying the original lattice framework. Hydrogen ions accumulate largely at the interfacial regions with amorphous character which extend about one-third of the total thickness. The H_xSrCrO_3 (HSCO) thin films appear like exfoliated layers which however retain the fully strained state with distorted perovskite structure. Proton doping induces the change of Cr oxidation state from Cr^{4+} to Cr^{3+} in HSCO thin films and a transition from metallic to insulating phase. Our investigations suggest an attractive platform in manipulating the electronic phases in proton-based approaches and may offer a potential peeling off strategy for nanoscale devices through low-energy hydrogen plasma implantation approaches.

Keywords transition metal oxide thin film, metal–insulator transition, hydrogenation

1 Introduction

Functional materials have attracted significant interests due to their novel electronic, photonics behaviors over the past decades [1–3]. Strongly correlated $3d$ transition metal oxides are characterized by the interplay of spin, charge, orbital degrees of freedom of the valence electrons, where a burst of strategies are proposed to manipulate their intimate couplings and uncover new functionalities [4, 5]. Among them doping exhibits as a controlling parameter with notable characters, e.g., the entering to superconducting state in high T_c superconductors [6]; the appearance of versatile ground states including the ferromagnetic metallic phase associated with colossal magnetoresistance in manganites [7]; the development of high concentrated n/p-type carries for electronic and optoelectronic devices [8]; the new emergent properties across the interface between various iso-structural compounds via interfacial structural proximity effect [9], etc..

The doping of hydrogen ion into transition metal oxides is unique due to the bonding flexibility, which can be forms of different types of charge states, i.e., positively charged proton H^+, or negatively charged hydride ion H^-, or charge neutral H^0 as reported in metallic hydrides. The introduction of hydride ion H^- in transition metal oxides, namely transition metal oxyhydride, has been reported to create a heavily n-type doped sys-

tem in $BaTiO_{3-x}H_x$ [10], to form the special M-H^--M bonds (M denoting the transition metal ions) resulting in an antiferromagntic ground state with high Neel temperatures in $SrVO_2H$, $LaSrCoO_3H_{0.7}$ and $SrCrO_2H$ compounds [11–14]. The protonation of transition metal complexes attracts considerable attentions, accompanying with the tunability of physical properties and the emergent novel electronic phases. For instance, the new $HSrCoO_{2.5}$ insulating ferromagnetic phase emerged in electric-field controlled insertion/extraction of H^+ ions in strontium cobaltite thin film via ionic liquid gating method [15]; the proton ion concentration controlled insulating (pristine)-metal-insulating phase modulation in VO_2 films through hydrogen spillover method [16]. Proton doping thus serves as an attractive strategy showing the capabilities in strong modulations of the crystal structures and the phase diagrams as well as in exploring novel electronic phases. Different protonation methods have been reported in literatures, e.g., the Pt-catalyst-assisted hydrogen spillover method [17], the different electrolyte gating methods [15, 16, 18], and the hydrogen bombardment method with several keV to MeV high energy hydrogen ion irradiation [19]. These protonation processes involve either time-consuming or chemical reaction or high energy ion irradiation environments which restrict the realist technological applications. Therefore, the search for an alternative nondestructive and efficient approach is demanding.

In this article, we demonstrate the protonation in $SrCrO_3$ (SCO) films using an elaborated low-energy hydrogen plasma implantation method. Hydrogen ions are incorporated into the SCO thin films avoiding the damage of the original lattice structure and accumulate largely at the interfacial region near the substrate which shows amorphous character. The protonated films (H_xSrCrO_3, or HSCO) appear analogous to exfoliated layers from the substrate which interestingly remain strained by the substrates with a strongly distorted perovskite crystal structure and a big lattice expansion of the out-of-plane lattice constant [as illustrated in Fig. 1(c)]. A band-filling controlled metal (SCO) to insulator (HSCO) transition has been proposed to SCO films upon protonation, associated with the variation of Cr electronic configuration from mainly Cr $3d^2$ to Cr $3d^3$ as determined from soft X-ray absorption measurements at Cr L_{23}-edge. Detailed configuration interaction (CI) cluster calculations have been performed to explore the multiplet features of HSCO films, which reinforce the existence of Cr^{3+} with a $3d^3$ electronic configuration of octahedral symmetry.

2 Experimental section

Bulk SCO shows a cubic perovskite structure with a lattice constant of 3.819Å as shown in Fig. 1(a), and adopts a Cr $3d^2$ electronic configuration in the ionic limit [20]. The electronic and magnetic properties of SCO are still under debates, which was reported as a paramagnetic metal originally [21], or a paramagnetic insulator owing to bond length fluctuations based on transport measurement [22], or an antiferromagnetic ground state attributed to orbital ordering based on neutron diffraction analysis [23]. Our SCO thin films were deposited on the compressively strained $LaAlO_3$ (001) (LAO) substrate by molecular beam epitaxial (MBE) technique followed by annealing in air at 250°C for $2h$, which show a fully-strained single crystalline phase with high quality from X-ray diffraction and transmission electron microscopy (TEM) analyses (see Ref. [20] for details) as well as a metallic paramagnetic ground state [24].

The hydrogenation experiments of epitaxial SCO thin films were performed with a home-made plasma facility where an adopted low-frequency inductively coupled plasma system was used to generate high density hydrogen

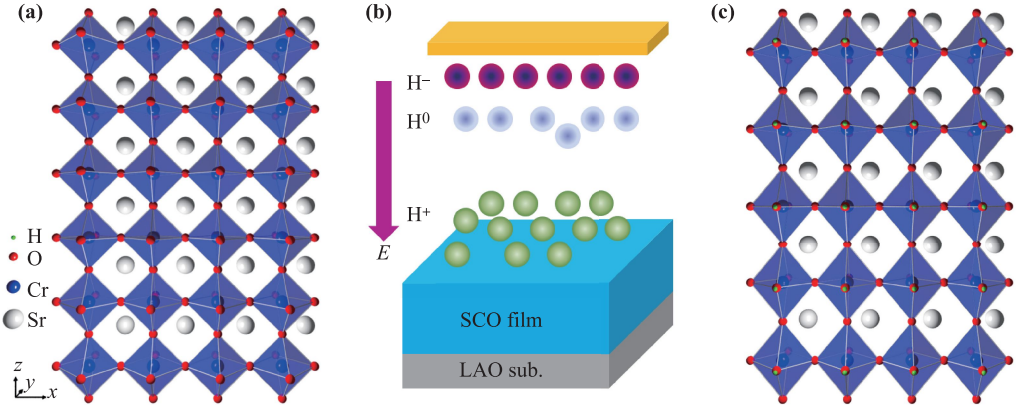

Fig. 1 Schematic views of **(a)** perovskite SCO with a cubic crystal structure which are formed by edge-sharing CrO_6 octahedra surrounding by Sr cations, **(b)** the low-energy hydrogen plasma implantation process with an applied dc bias to provide a dominant accumulation of protons near the film surface, and **(c)** the HSCO crystal structure after hydrogen plasma implantation with a lattice expansion of the out-of-plane lattice constant.

Table 1 Lists of experimental parameters for low-energy hydrogen plasma implantation measurements.

Pressure (Pa)	Temperature (°C)	RF power (W)	Flux (sccm)	Bias (V)	Treated time (min)
5	300	1800	20	−180	10

plasma [25]. Plasma is a quasineutral medium with identical densities of positive and negative particles. A negative *dc* bias of −180 V was applied to control the built-in electric field of the plasma, leading to a dominant accumulation of protons, rather than H^- or H^0, near the film surface as illustrated in Fig. 1(b). The hydrogen plasma implantation were carried out at a vacuum pressure of $5P_a$ and a base temperature of 300°C. The hydrogen plasma treatment was optimized with a RF power of 1800 W, H_2 fluxes of 20 sccm, and a treated time of 10 mins, as tabulated in Table 1. The plasma environment has been demonstrated as an attractive platform for synthesis of functional nanostructured materials [26, 27] which can be used for electronic, energy and space technological applications [28–30]. We note that our plasma treatment is a low-energy implantation and diffusion process of the ionized hydrogen gas with less destructive to the samples [25, 31], compared to the high-energy, high-flux plasma implantation in regular semiconductor techniques [32].

TOF-SIMS (time-of-flight secondary-ion mass spectrometry setup from GmbH, Germany) measurements had been performed to provide direct information about hydrogen concentrations. Caesium ion beam was used as the sputtering beam with energy of 1 keV at an incident angle of 45° and a sputtering rate of about 0.142 nm/s calibrated for SiO_2, which is capable for collecting the ions with atomic mass between 0–1000 amu. Taking into account the total thickness of SCO thin films as 50 nm, we estimate a sputtering rate of about 0.1 nm/s for SCO thin films. The depth profiles of different ions are shown in the main text. The atomic structures of HSCO thin films were examined using the JEOL2100F equipment for high resolution TEM measurements. The valence state of Cr is investigated by element-specific X-ray absorption measurements, where the positions of the absorption edges reflect the valence states directly. The absorption measurements were performed at the Magnetic Circular Dichroism beamline (BL12B) of National Synchrotron Radiation Laboratory (NSRL), Hefei. Data are collected in total electron yield mode.

3 Results and discussion

Figure 2(a) shows the θ–2θ X-ray diffraction near the LAO (002) reflection to determine the structural variation before and after hydrogen plasma implantation. The HSCO thin film shows a larger out-of-plane lattice constant of 3.973 ± 0.007 Å compared to 3.829 ± 0.005 Å of pristine SCO. The lattice expansion of the out-of-plane lattice constant is similar to the lattice expansion reported in protonated $HSCoO_{2.5}$ and HVO_2 systems, whereas opposite to the structural contraction observed in many transition-metal oxyhydrides with the replacement of O^{2-} by H^- anion, e.g., $LaSrCoO_3H_{0.7}$, $BaTiO_{3-x}H_x$, $SrCoO_xH_y$, and $SrVO_2H$ [10–13], etc.. The HSCO thin films preserve the perovskite crystal structure (as also suggested by the diffraction patterns from high resolution TEM shown in Figs. 3(c, d) where the HSCO film shows the same symmetry as the LAO substrate) and the fully strained state with identical in-plane lattice constant of 3.789 Å as LAO substrate from the reciprocal space maps around (103) reflections shown in Fig. 2(b). The lattice constant ratio $c/a \sim 1.048$ representing the tetragonality of HSCO film

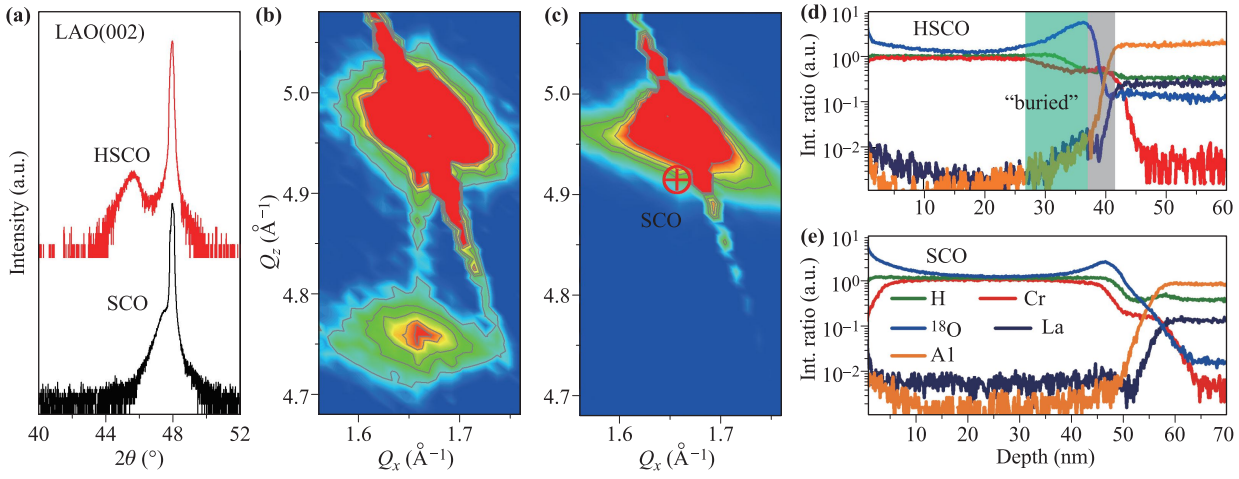

Fig. 2 **(a)** High resolution X-ray diffraction scans along the (002) direction for the investigated thin films. Panels **(b)** and **(c)** show the corresponding reciprocal space maps around (103) reflection index for HSCO and SCO thin films, respectively. **(d)** Intensity ratios for H, Cr, ^{18}O, La and Al ions in SIMS measurements of HSCO film and **(e)** a compared pristine SCO film with depth profiles.

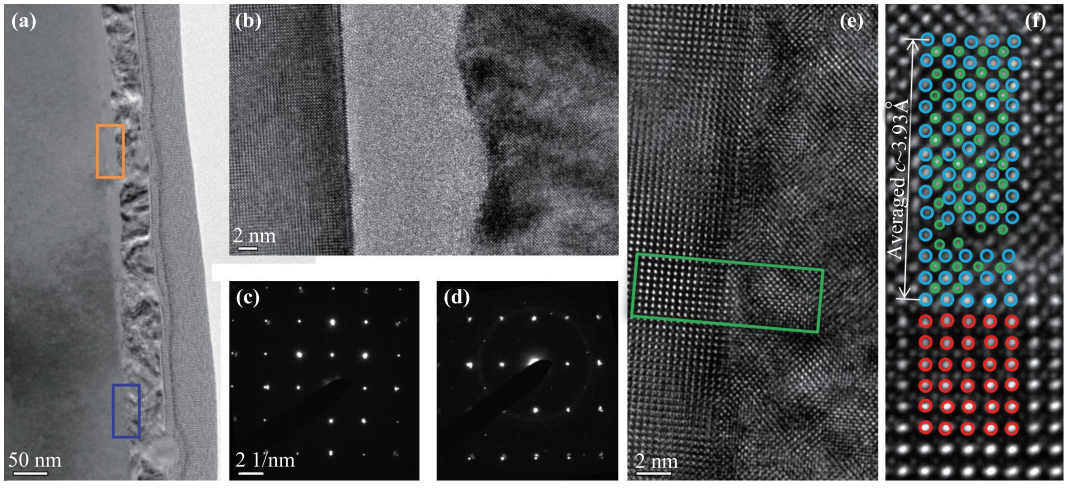

Fig. 3 **(a)** Bright field image of the HSCO thin films along (001) direction. **(b)** High resolution TEM image at interface with amorphous feature labelled as the orange rectangular shown in panel (a). **(c, d)** show the diffraction patterns for both HSCO film and LAO substrate along (001) and along (111) directions, respectively. **(e)** focuses on the blue interfacial region as marked in panel (a) showing a matched crystal structure, and panel **(f)** is the zoom in view of the green rectangular region.

is much larger than the $c/a \sim 1.01$ before treatment. The change of the crystal structure from cubic to tetragonal symmetry is illustrated in Figs. 1(a) and (c). This suggests the constraint of the in-plane biaxial lattice parameters by compressive strain induced by the substrate whereas only a strong expansion of the out-of-plane lattice constant is accommodated by hydrogen incorporation.

The insertion of hydrogen ions is verified by TOF-SIMS measurements. Since the absolute intensity values are meaningless, the intensity ratios [i.e., $I(\mathrm{A})/I(\mathrm{Cr})$ with A denoting H, Cr, ^{18}O, La and Al ions] are used for comparison and a pristine SCO film is used as reference. Figures 2(d, e) present the intensity ratios for different ions with depth profiles. Overall, hydrogen occupies both the thin films layer and to some extent in the substrate layers and the thin films there appears a reduction of the total thickness of $\sim$ 12 nm after ion implantation experiment which might be related to the small amount of plasma etching at the surface region. A pronounced hydrogen content is observed for HSCO film compared to pristine SCO, confirming the existence of hydrogen through implantation experiment. The hydrogen ions show accumulations at the interfacial region near the LAO substrate. Moreover, Cr ion exhibits a reduced intensity at the H accumulated region close to the interface, which is further identified as "buried" areas without well-defined crystallinity from high resolution TEM measurements as shown in Fig. 3. Finally, no clear oxygen vacancies is observed before and after hydrogen plasma implantation as suggested by the comparable normalized $I(^{18}\mathrm{O})/I(\mathrm{Cr})$ intensities, implying that proton incorporation rather than the creation of oxygen deficiencies is the main reason for the variation of electronic configurations as will be presented below.

Subsequent structural analysis of HSCO films with high resolution TEM measurements are shown in Fig. 3. The thickness of the thin film is about 50 nm, as suggested from the bright field TEM image in Fig. 3(a). More than two-thirds of the interfacial regions with hydrogen accumulations exhibit amorphous feature without well-defined crystallinity. The "buried" regions expand about 10 nm in thickness as determined from the high resolution TEM image in Fig. 3(b). The low connectivity of the structural blocks at the interfacial region and the easy solubility feature of amorphous phase compared to solid phase with ionic bonds provide the possibility to be peeled off from the substrate which might allow for the capability to be transferred to other substrates flexibly. The HSCO thin films appear like exfoliated layers which however retain the fully strained state with the same in-plane lattice constant as the substrate as suggested by off-specular reciprocal space map and the similar crystal symmetry as suggested by the TEM diffraction patterns along (001) and (111) directions [Figs. 3(c, d)]. Figure 3(e) shows the high resolution TEM image at the interface between the HSCO and LAO substrates corresponding to the small region without amorphous character as marked in panel (a). The rectangular area is enlarged in Fig. 3(f) showing a good epitaxial relationship between the HSCO film and the LAO substrate, which however shows some missing of atoms near the interfacial region. The atomic positions of the heavy ions indicate a strongly distorted perovskite structure which might be related to the change of the radii of transition metal ion due to the change of valence state from Cr^{4+} to Cr^{3+} and the interstitial of protons with attractive force to the negatively charge O^{2-} ions. The averaged out-of-plane lattice constant of the HSCO film is estimated to be $\sim$ 3.93 Å as shown in Fig. 3(f), which is consistent with the out-of-plane lattice constant expansion determined from X-ray diffraction measurements.

Figure 4(a) displays the Cr L_{23}-edge absorption spectra

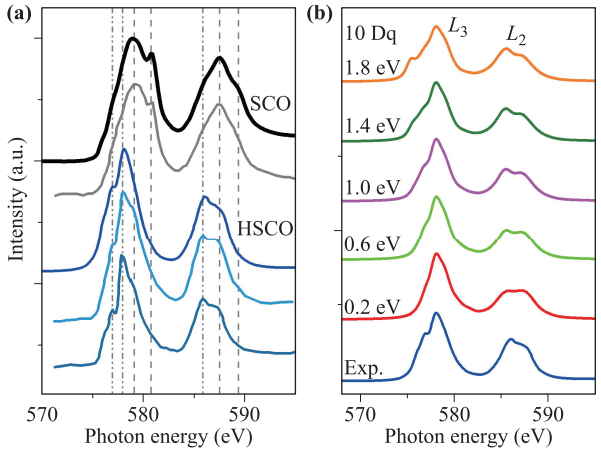

Fig. 4 **(a)** X-ray absorption spectra at Cr L_{23}-edge for the measured SCO sample, the SCO thin film reported in literature, the measured HSCO film after hydrogen plasma implantation, the measured $SrCrO_{2.8}$ thin film with oxygen deficiencies and the $LaCrO_3$ thin film from top to bottom [33, 34]. **(b)** Isotropic spectra with different crystal field splitting energies 10 Dq from 0.2 eV to 1.8 eV obtained from CI calculations in comparison with the experimental measured absorption spectrum for HSCO films.

of SCO and HSCO thin film. The Cr L_{23}-edge absorption spectra compose of Cr L_3 and L_2 edges owing to spin-orbit coupling of the Cr $2p$ levels. The pristine SCO film shows identical absorption spectra as the SCO film reported in literature in both Cr L_{23}-edge and O K-edge [as shown in Fig. 5(b)], suggesting a mainly Cr^{4+} valence state. The peak positions at Cr L_{23}-edge of HSCO films exhibit a shift of approximately 1.15 eV towards lower absorption energies compared to pristine phase, which is a comparable chemical shift as reported in literatures for one electron change in Cr ions and indicates the primarily Cr^{3+} valence state [20]. We further compare the measured absorption spectra to the reference spectra measured in oxygen-deficient $SrCrO_{2.8}$ thin films and the spectra reported in literatures for SCO thin film [20], the $La_{0.75}Sr_{0.25}CrO_3$ and the $LaCrO_3$ thin films [33, 34]. The HSCO film show comparable absorption edges as the $La_{0.75}Sr_{0.25}CrO_3$ and $LaCrO_3$ thin films with the dominant Cr^{3+} valence state.

To obtain a deep insight into the electronic information of Cr L_{23}-edge X-ray absorption spectrum, we perform the configuration interaction (CI) cluster calculation for a CrO_6 (Cr: $3d^3$) cluster with $3d^3$ electronic configuration. CI cluster calculations take the full multiplet effects into account and show the advantages of interpreting the L_{23}-edge excitation spectrum over the last decades [35–37]. We refer to the literatures as well as our previous reports for the backgrounds and details on performing the CI cluster calculations [35, 37–39]. The simulated spectra presented here are considered only the three lowest energy configurations. The simulated spectra are shown in Fig. 4(b) with a variation of the crystal splitting energy 10 Dq from 0.2 eV to 1.8 eV at an interval of 0.4 eV. The other energy parameters used for present calculations are (in units of eV): $U_{dd} = 5.5$, $U_{pd} = 7.3$, $\Delta = 5.5$, $pd\sigma = 2$, which are the same as the values used in $LaCrO_3$ and Cr_2O_3 compounds [40, 41]. As 10 Dq increases, the peak splitting inside the L_3 and L_2 absorption edges increases due to the increased energy differences between the t_{2g} and e_g levels. A further comprehensive comparison between the energy splitting values at Cr L_3 edge and the intensity ratios at Cr L_2 excitation peaks suggests a 10 Dq value between 1.0 and 1.4 eV which reproduces the experimental spectrum well. Our CI calculations further reinforce that the Cr ions exist with 3+ valence state sharing an octahedral symmetry surrounded by six O atoms in HSCO thin films, whereas Cr with other valence states are not favorable.

A combined valence band X-ray photoelectron spectroscopy (VB XPS) and O K-edge absorption measurements have been performed to investigate the variation of electronic structures close to Fermi level. The valence band XPS spectra are shown in Fig. 5(a), all of which are referenced to the Fermi level using a Au foil with direct electronic contact to the film surface for energy calibration. The VB XPS spectra are characterized by three regions labelled as A_1, A_2 and A_3. The two peaks showing high binding energies relative to the Fermi level (A_2 and A_3) are dominated by the O $2p$-derived with minor Cr contributions due to the O $2p$-Cr $3d$ hybridization. Peak A_1 close to the Fermi level can be assigned to the occupied Cr $3d$ t_{2g} orbitals with a high-spin electronic configuration. The assignments of these features are the same as been proposed for SCO films, $LaCrO_3$ powder and thin films as well as the band structure calculations by density functional theory therein [33, 34, 42]. A notable variation of the density of states near the Fermi level has been suggested from valence band XPS spectra. In the pristine SCO film, the Fermi level lies inside the Cr $3d$ band, which is consistent with the metallic electrical conductivity behavior [33] and is expected due to the partially occupied electronic states on the six-fold degenerated t_{2g} manifold. However, the valence band maximum is located below the Fermi level for HSCO films, indicating the formation of a band gap after hydrogen plasma implantation, as will be discussed below.

The multiplet structures at O K-edge show dramatic different Cr d-O p hybridization characters for Cr^{4+} and Cr^{3+}, as shown in Fig. 5(b). The peaks B_1-B_4 in SCO film can be assigned to the excitations to empty $Crt_{2g}\uparrow$ $t_{2g}\downarrow$ $e_g\uparrow$ $e_g\downarrow$ states, associated with a metallic state. The O K-edge absorption spectrum of HSCO thin film shows a higher excitation energies which is comparable to that of oxygen deficient $SrCrO_{2.8}$ film, but with less spectral features at the Cr-O hybridization region compared to others. The loss of hybridisation feature is similar to the results observed in $HSrCoO_{2.5}$ and Li_xFeO_4 upon lithiation [15, 43].

In the ionic limit, pristine SCO has a t_{2g}^2 electronic configuration where the e_g electron levels are higher in en-

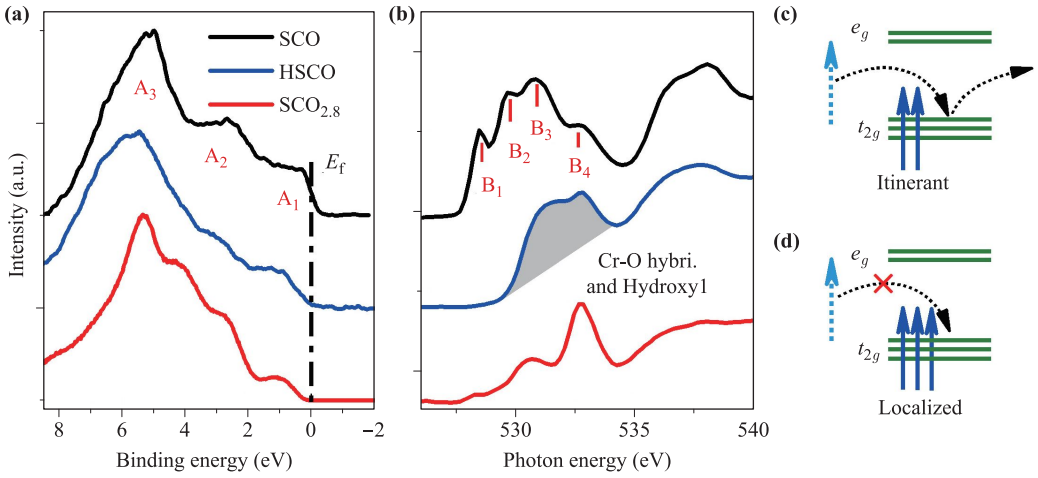

Fig. 5 **(a, b)** The valence band XPS spectra and O K-edge absorption spectra for SCO film, HSCO film after hydrogen plasma implantation and oxygen deficient $SCO_{2.8}$ film. Schematic illustrations of the electronic configurations for **(c)** pristine SCO and **(d)** proton-doped HSCO systems in the ionic limit.

ergies due to crystal field effect. The small bond length differences between in-plane and out-of-plane directions as well as the small on-site energy differences among d_{xy}, d_{xz} and d_{yz} orbitals result in a metallic ground state in pristine SCO, where the two electrons are shared by three orbitals in t_{2g} level. An electron itinerant model as illustrated in Fig. 5(c) thus is expected due to the unoccupied electronic states on the six-fold degenerated t_{2g} manifold, which agrees well with the presence of density of states near Fermi level as suggested by VB XPS spectrum. The HSCO thin films are transparent in color and are insulators with room temperature resistance above 5 MΩ. The absence of density of states near Fermi level for HSCO film is similar to that of the oxygen deficient $SCO_{2.8}$ phase which shows an insulating behavior. Doping of protons induces a single electron to Cr ion with Cr valence state changing from Cr^{4+} to Cr^{3+} as confirmed in the Cr L_{23}-edge absorption measurements. Cr^{3+} in HSCO films adopts the t_{2g}^3 electronic configuration. An energy gap is expected, where an energy barrier should be suppressed for electronic conductivity. Band filling of 3d orbitals is one of the main concepts in strongly correlated systems, which determines various electronic ground phases [7]. The metal (SCO)-insulator (HSCO) transition is analogous to the band-filling controlled Mott transitions through proton doping effect, similar as reported in proton-doped $SmNiO_3$ compound [44]. Moreover, the strongly distorted structure might also contribute to the insulating behavior due to the reduced bandwidth with strong distorted Cr-O-Cr bonds.

4 Conclusions

In conclusion, an efficient and nondestructive low-energy hydrogen plasma implantation experiment has been elaborated to investigate the H accumulation effect and the modulation of the electronic phases in transition metal SCO thin films. Hydrogen ions accumulate largely at the interfacial regions near the LAO substrate. The atomic structure at the interfacial region is examined by high resolution TEM measurements which shows amorphous character. The low connectivity of the structural blocks at the interfacial region and the easy solubility feature of amorphous phase compared to solid phase with ionic bonds suggest that the HSCO films are convenient to peel off and allow to be transferred to other substrates flexibly, which however retain the fully strained state with distorted perovskite structure. Proton introduces an additional electron to the strontium chromium thin films which induces a mainly Cr^{3+} valence state in HSCO films compared to the primarily Cr^{4+} in pristine SCO films. The variation of the electronic configuration from $3d^2$ to $3d^3$ upon protonation drives a change from metallic (SCO) to insulating (HSCO) phases as suggested by the variation of the density of states near Fermi level from VB XPS characterizations, analogous to the band-filling controlled Mott transition mechanism. The multiplet features at Cr L_{23}-edge absorption spectrum of HSCO film can be reproduced well with crystal field splitting 10 Dq between 1.0–1.4 eV using CI cluster calculations considering the Cr t_{2g}^3 electronic configuration of a CrO_6 cluster under octahedral symmetry. This implies the retain of the original crystal structures which avoids the strong disorder of Cr ions due to hydrogen bombardment or the occupancy of the substitutional sites by hydrogen ions rather than interstitial sites. The facile hydrogenation process offers a new possibility to tailor the crystal structure and the electronic configurations towards fascinating physical properties of perovskite oxides, such as hydrogen storage devices as well as integrated electronic and photonic applications [45, 46]. The special interfacial properties between

the thin film and the substrate may pave a new strategy for application of strain-mediated transition metal oxide thin films towards nanoscale engineering through peeling off process, and open a new platform to manipulate the interplay between different collective phenomena through non-destructive low-energy hydrogen plasma implantation approach.

Acknowledgements We acknowledge the valuable discussion with X. P. Yang and the provision of synchrotron radiation at NSRL. This project was funded by National Natural Science foundation of China (Grant No. 11704317) and China Postdoctoral Science Foundation (Grant No. 2016M602064). We also acknowledge the supports by the Natural Science Foundation of Shenzhen University (Grant No. 827-000198). Epitaxial film growth and characterization were supported by the U. S. Department of Energy (DOE), Office of Basic Energy Sciences, Division of Materials Science and Engineering under award No. 10122 and was carried out at the W. R. Wiley Environmental Molecular Sciences Laboratory, a DOE User Facility sponsored by the Office of Biological and Environmental Research at PNNL, a multi-program national laboratory operated for DOE by Battelle.

References

1. J. L. Zhang and G. C. Shan, Stacking control in graphene-based materials: A promising method for fascinating physical properties, *Front. Phys.* 14(2), 23301 (2019)
2. T. Chatterji, S. Rols, and U. D. Wdowik, Dynamics of the phase-change material GeTe across the structural phase transition, *Front. Phys.* 14(2), 23601 (2019)
3. R. Wang, X. G. Ren, Z. Yan, L. J. Jiang, W. E. I. Sha, and G. C. Shan, Graphene based functional devices: A short review, *Front. Phys.* 14(1), 13603 (2019)
4. S. Q. Luo, J. F. Wang, B. Yang, and Y. B. Yuan, Recent advances in controlling the crystallization of two-dimensional perovskites for optoelectronic device, *Front. Phys.* 14(5), 53401 (2019)
5. T.-H. Han, S. Tan, J. Xue, L. Meng, J.-W. Lee, and Y. Yang, Interface and defect engineering for metal halide perovskite optoelectronic devices, *Adv. Mater.* 1803515 (2019)
6. M. R. Norman, The challenge of unconventional superconductivity, *Science* 332(6026), 196 (2011)
7. M. Imada, A. Fujimori, and Y. Tokura, Metal-insulator transitions, *Rev. Mod. Phys.* 70(4), 1039 (1998)
8. J. M. D. Coey, M. Venkatesan, and C. B. Fitzgerald, Donor impurity band exchange in dilute ferromagnetic oxides, *Nat. Mater.* 4(2), 173 (2005)
9. H. Y. Hwang, Y. Iwasa, M. Kawasaki, B. Keimer, N. Nagaosa, and Y. Tokura, Emergent phenomena at oxide interfaces, *Nat. Mater.* 11(2), 103 (2012)
10. Y. Kobayashi, O. J. Hernandez, T. Sakaguchi, T. Yajima, T. Roisnel, Y. Tsujimoto, M. Morita, Y. Noda, Y. Mogami, A. Kitada, M. Ohkura, S. Hosokawa, Z. Li, K. Hayashi, Y. Kusano, J. Kim, N. Tsuji, A. Fujiwara, Y. Matsushita, K. Yoshimura, K. Takegoshi, M. Inoue, M. Takano, and H. Kageyama, An oxyhydride of $BaTiO_3$ exhibiting hydride exchange and electronic conductivity, *Nat. Mater.* 11(6), 507 (2012)
11. M. A. Hayward, E. J. Cussen, J. B. Claridge, M. Bieringer, M. J. Rosseinsky, C. J. Kiely, S. J. Blundell, I. M. Marshall, and F. L. Pratt, The hydride anion in an extended transition metal oxide array: $LaSrCoO_3H_{0.7}$, *Science* 295(5561), 1882 (2002)
12. F. Denis Romero, A. Leach, J. S. Möller, F. Foronda, S. J. Blundell, and M. A. Hayward, Strontium vanadium oxide-hydrides: "Square-planar" two-electron phases, *Angew. Chem. Int. Ed.* 53(29), 7556 (2014)
13. C. Tassel, Y. Goto, Y. Kuno, J. Hester, M. Green, Y. Kobayashi, and H. Kageyama, Direct synthesis of chromium perovskite oxyhydride with a high magnetic-transition temperature, *Angew. Chem. Int. Ed.* 53(39), 10377 (2014)
14. Y. Kobayashi, O. Hernandez, C. Tassel, and H. Kageyama, New chemistry of transition metal oxyhydrides, *Sci. Technol. Adv. Mater.* 18(1), 905 (2017)
15. N. Lu, P. Zhang, Q. Zhang, R. Qiao, Q. He, H. B. Li, Y. Wang, J. Guo, D. Zhang, Z. Duan, Z. Li, M. Wang, S. Yang, M. Yan, E. Arenholz, S. Zhou, W. Yang, L. Gu, C. W. Nan, J. Wu, Y. Tokura, and P. Yu, Electric-field control of tri-state phase transformation with a selective dual-ion switch, *Nature* 546(7656), 124 (2017)
16. M. Jo, H. J. Lee, C. Oh, H. Yoon, J. Y. Jo, and J. Son, Gate-induced massive and reversible phase transition of VO_2 channels using solid-state proton electrolytes, *Adv. Funct. Mater.* 28(39), 1802003 (2018)
17. H. Yoon, M. Choi, T. W. Lim, H. Kwon, K. Ihm, J. K. Kim, S. Y. Choi, and J. Son, Reversible phase modulation and hydrogen storage in multivalent VO_2 epitaxial thin films, *Nat. Mater.* 15(10), 1113 (2016)
18. M. A. Hope, K. J. Griffith, B. Cui, F. Gao, S. E. Dutton, S. S. P. Parkin, and C. P. Grey, The role of ionic liquid breakdown in the electrochemical metallization of VO_2: An NMR study of gating mechanisms and VO_2 reduction, *J. Am. Chem. Soc.* 140(48), 16685 (2018)
19. K. A. Smith, A. I. Savva, C. Deng, J. P. Wharry, S. Hwang, D. Su, Y. Wang, J. Gong, T. Xu, D. P. Butt, and H. Xiong, Effects of proton irradiation on structural and electrochemical charge storage properties of TiO_2 nanotube electrodes for lithium-ion batteries, *J. Mater. Chem. A* 5(23), 11815 (2017)
20. K. H. L. Zhang, P. V. Sushko, R. Colby, Y. Du, M. E. Bowden, and S. A. Chambers, Reversible nanostructuring of $SrCrO_{3-d}$ through oxidation and reduction at low temperature, *Nat. Commun.* 5(1), 4669 (2014)
21. B. L. Chamberland, Preparation and properties of $SrCrO_3$, *Solid State Commun.* 5(8), 663 (1967)
22. J. S. Zhou, C. Q. Jin, Y. W. Long, L. X. Yang, and J. B. Goodenough, Anomalous electronic state in $CaCrO_3$ and $SrCrO_3$, *Phys. Rev. Lett.* 96(4), 046408 (2006)

23. L. Ortega-San-Martin, A. J. Williams, J. Rodgers, J. P. Attfield, G. Heymann, and H. Huppertz, Microstrain sensitivity of orbital and electronic phase separation in $SrCrO_3$, *Phys. Rev. Lett.* 99(25), 255701 (2007)
24. K. H. L. Zhang, Y. Du, P. V. Sushko, M. E. Bowden, V. Shutthanandan, L. Qiao, G. Cao, Z. Gai, S. Sallis, L. Piper, and S. A. Chambers, Electronic and magnetic properties of epitaxial perovskite $SrCrO_3$(001), *J. Phys.: Condens. Matter* 27(24), 245605 (2015)
25. H. P. Zhou, X. Ye, W. Huang, M. Q. Wu, L. N. Mao, B. Yu, S. Xu, I. Levchenko, and K. Bazaka, Wearable, flexible, disposable plasma-reduced graphene oxide stress sensors for monitoring activities in austere environments, *ACS Appl. Mater. Interfaces* 11(16), 15122 (2019)
26. I. Levchenko, K. Bazaka, M. Keidar, S. Xu, and J. Fang, Hierarchical multicomponent inorganic metamaterials: Intrinsically driven self-assembly at the nanoscale, *Adv. Mater.* 30(2), 1702226 (2018)
27. O. Baranov, I. Levchenko, J. M. Bell, J. W. M. Lim, S. Huang, L. Xu, B. Wang, D. U. B. Aussems, S. Xu, and K. Bazaka, From nanometre to millimetre: A range of capabilities for plasma-enabled surface functionalization and nanostructuring, *Mater. Horiz.* 5(5), 765 (2018)
28. I. Levchenko, K. Bazaka, T. Belmonte, M. Keidar, and S. Xu, Advanced materials for next-generation spacecraft, *Adv. Mater.* 30(50), 1802201 (2018)
29. I. Levchenko, S. Xu, G. Teel, D. Mariotti, M. L. R. Walker, and M. Keidar, Recent progress and perspectives of space electric propulsion systems based on smart nanomaterials, *Nat. Commun.* 9(1), 879 (2018)
30. I. Levchenko, M. Keidar, J. Cantrell, Y.L. Wu, H. Kuninaka, K. Bazaka, and S. Xu, Explore space using swarms of tiny satellites, *Nature* 562(7726), 185 (2018)
31. H. P. Zhou, D. Y. Wei, S. Xu, S. Q. Xiao, L. X. Xu, S. Y. Huang, Y. N. Guo, S. Khan, and M. Xu, Crystalline silicon surface passivation by intrinsic silicon thin films deposited by low-frequency inductively coupled plasma, *J. Appl. Phys.* 112(1), 013708 (2012)
32. M. Losurdo, P. Capezzuto, G. Bruno, and E. A. Irene, Chemistry and kinetics of the GaN formation by plasma nitridation of GaAs: An *in situ* real-time ellipsometric study, *Phys. Rev. B* 58(23), 15878 (1998)
33. K. H. L. Zhang, Y. Du, P. V. Sushko, M. E. Bowden, V. Shutthanandan, S. Sallis, L. F. J. Piper, and S. A. Chambers, Hole-induced insulator-to-metal transition in $La_{1-x}Sr_xCrO_3$ epitaxial films, *Phys. Rev. B* 91(15), 155129 (2015)
34. D. D. Sarma, K. Maiti, E. Vescovo, C. Carbone, W. Eberhardt, O. Rader, and W. Gudat, Investigation of hole-doped insulating $La_{1-x}Sr_xCrO_3$ by soft-X-ray absorption spectroscopy, *Phys. Rev. B* 53(20), 13369 (1996)
35. G. van der Laan, J. Zaanen, G. A. Sawatzky, R. Karnatak, and J. M. Esteva, Comparison of X-ray absorption with X-ray photoemission of nickel dihalides and NiO, *Phys. Rev. B* 33(6), 4253 (1986)
36. M. W. Haverkort, M. Zwierzycki, and O. K. Andersen, Multiplet ligand-field theory using Wannier orbitals, *Phys. Rev. B* 85(16), 165113 (2012)
37. M. W. Haverkort, Quanty - a quantum many body script language, 2016
38. M. Wu, H. L. Xin, J. O. Wang, X. J. Li, X. B. Yuan, H. Zeng, J. C. Zheng, and H. Q. Wang, Investigation of the multiplet features of $SrTiO_3$ in X-ray absorption spectra based on configuration interaction calculations, *J. Synchrotron Radiat.* 25(3), 777 (2018)
39. M. Wu, J. C. Zheng, and H. Q. Wang, Investigation of the vanadium L_{23}-edge X-ray absorption spectrum of $SrVO_3$ using configuration interaction calculations: Multiplet, valence, and crystal-field effects, *Phys. Rev. B* 97(24), 245138 (2018)
40. T. Saitoh, A. E. Bocquet, T. Mizokawa, and A. Fujimori, Systematic variation of the electronic structure of 3 *d* transition-metal compounds, *Phys. Rev. B* 52(11), 7934 (1995)
41. A. E. Bocquet, T. Mizokawa, K. Morikawa, A. Fujimori, S. R. Barman, K. Maiti, D. D. Sarma, Y. Tokura, and M. Onoda, Electronic structure of early 3*d*-transition-metal oxides by analysis of the 2*p* core-level photoemission spectra, *Phys. Rev. B* 53(3), 1161 (1996)
42. J. Suntivich, W. T. Hong, Y. L. Lee, J. M. Rondinelli, W. Yang, J. B. Goodenough, B. Dabrowski, J. W. Freeland, and Y. Shao-Horn, Estimating hybridization of transition metal and oxygen states in perovskites from O*K*-edge X-ray absorption spectroscopy, *J. Phys. Chem. C* 118(4), 1856 (2014)
43. X. Liu, Y. J. Wang, B. Barbiellini, H. Hafiz, S. Basak, J. Liu, T. Richardson, G. Shu, F. Chou, T. C. Weng, D. Nordlund, D. Sokaras, B. Moritz, T. P. Devereaux, R. Qiao, Y. D. Chuang, A. Bansil, Z. Hussain, and W. Yang, Why $LiFePO_4$ is a safe battery electrode: Coulomb repulsion induced electron-state reshuffling upon lithiation, *Phys. Chem. Chem. Phys.* 17(39), 26369 (2015)
44. Y. Zhou, X. Guan, H. Zhou, K. Ramadoss, S. Adam, H. Liu, S. Lee, J. Shi, D. D. Tsuchiya, M. Fong, and S. Ramanathan, Strongly correlated perovskite fuel cells, *Nature* 534(7606), 231 (2016)
45. S. J. Li, Y. T. Zhou, X. Kang, D. X. Liu, L. Gu, Q. H. Zhang, J. M. Yan, and Q. Jiang, A simple and effective principle for a rational design of heterogeneous catalysts for dehydrogenation of formic acid, *Adv. Mater.* 31(15), 1806781 (2019)
46. I. Abdelwahab, P. Dichtl, G. Grinblat, K. Leng, X. Chi, I. H. Park, M. P. Nielsen, R. F. Oulton, K. P. Loh, and S. A. Maier, Giant and tunable optical nonlinearity in single-crystalline 2D perovskites due to excitonic and plasma effects, *Adv. Mater.* 31(29), 1902685 (2019)